Science of Remote Sensing 7 (2023) 100077

Contents lists available at ScienceDirect

Science of Remote Sensing

journal homepage: www.sciencedirect.com/journal/science-of-remote-sensing

Brackish-water desalination plant modulates ground deformation in the city of Cape Coral, Florida

Gökhan Aslan [a,*], Ivanna Penna [a], Ziyadin Cakir [b], John Dehls [a]

[a] Geological Survey of Norway (NGU), Trondheim, Norway
[b] Department of Geological Engineering, Istanbul Technical University (ITU), Istanbul, Turkey

ARTICLE INFO

Keywords:
InSAR
Subsidence
BWRO
Desalination
Florida
Cape coral

ABSTRACT

The groundwater abstraction and injection cycle in coastal aquifer systems can locally change the piezometric head in aquifer system, leading to differential settlement on the ground that may compromise infrastructure safety. Furthermore, long-term, extensive groundwater extraction may cause significant damage to water resources. Ironically, Florida, a state known for its abundant water resources, has been experiencing major water supply issues in some areas that began to intensify with rapid population growth over the last five decades. As the demand for drinking water in Florida continues to rise, local authorities have turned to using brackish and saline water sources. As of 2022, more than 80% of the desalination plants in the United States are concentrated in the coastal areas of central and south Florida. Using satellite radar interferometry, we have investigated the spatiotemporal evolution of surface subsidence driven by groundwater pumping for brackish-water reverse osmosis (BWRO) desalination facilities in the City of Cape Coral, Florida. We employed Persistent Scatterer Interferometry (PSI) to process all available Sentinel 1A and 1B scenes over the region along two ascending orbits. The deformation time-series obtained from independent SAR data sets are compared spatiotemporally with the groundwater level that provides feed water to the BWRO facilities. The deformation pattern shows one main lobe of subsidence with rates of up to 25 mm/year centred around the operating wells in the north BWRO wellfield that we interpret as human-induced compaction. The spatial correlation between the subsiding area and the active production wells argues in favour of surface deformation induced by the BWRO operations. Based on the InSAR-derived displacement field and well data, we propose a model to explain the spatial heterogeneity of the subsidence process. The ground deformation is reproduced by an elastic model mimicking the reservoir compaction using planar negative closing dislocations. Modelling of the subsidence shows ~ 0.67 $Mm^3\ yr^{-1}$ vol loss due to compaction of the aquifer. The subsidence deformation was also used to compute the cumulative drainage area of the producing wells.

1. Introduction

According to the National Resources Defense Council (NRDC), Florida is one of the 14 states predicted to have an extreme or high risk in terms of water availability as demand exceeds sustainable supply by 2050 (Spencer and Altman 2010). Most of the state has historically relied on underground fresh water extracted from the Upper Floridan Aquifer (Miller 1990), one of the world's most prolific aquifers (Marella and Berndt 2005). However, because future increases in freshwater withdrawal will have a significant negative impact on the region's water resources, the aquifer alone was not capable of meeting the state's growing water demands (Miller 1990). In addition, given that Florida is one of the fastest-growing states in the United States, this puts tremendous pressure on conventional surface and groundwater resources. As a result, in the 1970s, the government began developing alternative water supply projects, including the use of seawater, brackish groundwater, surface water, stormwater, and reclaimed water to meet the constantly rising water needs. As of 2022, Florida leads the nation in the use of desalination technology to treat brackish water and seawater, with more than 130 desalination plants (Florida Department of Environmental Protection).

Most of Florida is underlain by a thick sequence of carbonate rock deposits (soluble limestone and dolomite) sculpted by dissolution and weathering processes (Tihansky 1999). The hummocky karst

* Corresponding author.
E-mail address: gokhan.aslan@ngu.no (G. Aslan).

https://doi.org/10.1016/j.srs.2023.100077
Received 4 October 2022; Received in revised form 19 January 2023; Accepted 20 January 2023
Available online 28 January 2023

topography of the state is characterised by the lack of a well-developed surface drainage system and the abundance of closed, shallow depressions, many of which are filled with water and are commonly associated with sinkhole development (Short and Blair 1986). While most sinkhole subsidence events in this region are attributed to natural karst processes, man-made activities, including well drilling, dewatering foundations and mining, can potentially facilitate the natural sinkhole formation process. A dramatic cause-and-effect relationship between aggressive groundwater pumping, hydraulic head decline and sinkhole development has been documented in several well fields in Florida (Sinclair 1982).

Given all these predisposing factors and the state's increasing dependence on groundwater extraction as its primary source of fresh water, ground deformation monitoring is crucial for predicting and mitigating subsidence hazards. The majority of hydrogeologic events directly contribute to the mass balance alteration and induce poroelastic media deformation that can be measured at the surface (Chaussard et al., 2014; Schuite et al., 2015; Castellazzi et al., 2016). Surface deformation caused by fluid pressure fluctuations in geological medium has been investigated using a variety of conventional and innovative techniques depending on the extent of the study area, including GNSS measurements, Interferometric Synthetic Aperture Radar (InSAR), tiltmeters and levelling. Several researchers have discussed the potential and limitations of these tools for hydrological surveys (Moreau and Dauteuil 2013; Castellazzi et al., 2016). Each geodetic technique provides different kinds of information and has its advantages, limitations, and application range. Compared to the traditional mapping approaches, InSAR is a very efficient tool for wide-area subsidence monitoring. Its use in hydrogeological surveys has been well documented in the world's major aquifers over the last decade, owing to its broad spatial coverage, high spatio-temporal resolution, and ability to operate in all weather conditions (Galloway and Hoffmann, 2007; Galloway 2014). There are currently three main InSAR processing methods employed in hydrogeological applications: Conventional Differential InSAR (D-InSAR), Small Baseline Subset (SBAS), and Persistent Scatterers Interferometry (PSI). The differential InSAR technique, in general, relies on the measurement of the deformation in a light-of-sight direction (LOS) by differencing the phase component of two (or more) coregistered SAR images acquired from slightly different orbital positions at different times (Pepe and Calò 2017). Ideally, the D-InSAR technique generates a high-density measured displacement field when the physical and geometrical nature of the scattering features remain nearly the same between two image acquisitions. However, even though the D-InSAR has significantly improved hydrogeologic characterisation of specific aquifers and advanced our understanding of hydrogeologic processes (Amelung et al., 1999; Galloway 2014), it is limited by temporal and geometrical decorrelation as well as atmospheric delay anomalies (Hanssen 2001). On the other hand, multi-temporal InSAR methodologies (SBAS and PSI) based on the analysis of stacks of SAR data retrieve surface displacement through time and eliminate most of the limitations related to D-InSAR (Crosetto et al., 2016). The PSI technique enables the detection of extremely slow ground deformation and is highly suitable for monitoring subsidence deformations in urban settings (Ferretti et al., 2001). InSAR-derived deformation results have been used to estimate hydromechanical properties of aquifers (Chaussard et al., 2014; Aslan et al., 2019; Peng et al., 2022), refine fault locations (Chaussard et al., 2014; Qu et al., 2015; Hu and Bürgmann 2020), simulate of groundwater flow and aquifer system compaction (Jafari et al., 2016) and simulate subsidence (Fernandez et al., 2018).

To our best knowledge, this is the first InSAR study revealing the ground deformation regulated by the desalination facility in the City of Cape Coral, Florida. Because the examined area is entirely urbanised, it will give high quality scattered targets over the study area. In the present study, we compute time series of deformation with the multitemporal PSI InSAR technique using Sentinel-1 A/B images acquired between 2015 and 2022. Our research relates the surface deformations obtained with InSAR to groundwater depletion induced by persistent groundwater pumping to feed the desalination facilities as well as the hydrogeological structure of the region. The primary goal of this study is to demonstrate how InSAR could be used effectively to estimate certain hydromechanical properties of aquifers and as an active data source during production and injection operations in desalination facilities. We describe the subsidence pattern observed over the desalination facility, quantify the associated ground deformation rates spatio-temporally, and suggest that such patterns are likely related to reservoir pumping and associated compaction.

2. Study area

The City of Cape Coral is a residential community in Lee County. It is the third-largest Florida city by landmass (310 km^2), with an estimated population of 210,000 as of the 2021 Census (U.S. Census United States Census Bureau, 2021). The city's population has steadily increased in the last 40 years, and the availability of traditional water sources, such as ground and surface water, has diminished. This has led to a movement toward developing environmentally sound alternative water supply sources, including brackish groundwater and seawater (Hill, 2012; Borisova et al., 2020). The South Cape Coral desalinisation facility, which started operating in 1976, is the oldest continuously operated BWRO plant in the United States, with a production capacity of 68,182 m^3/d (Pearson et al., 2021). The additional Reverse Osmosis (R.O.) plant started operating in 2010 with a capacity of 45,455 m^3/d in the northern part of the city (City of Cape Coral, Annual Consumer Report, 2019). With a total capacity of 113,637 m^3/d, the city's total potable water supply-demand is met by these two facilities (Harvey and Missimer 2020). Both BWRO facilities extract brackish groundwater from the Lower Hawthorn Aquifer, which is the uppermost part of the Floridan Aquifer System (Fig. 2; Missimer and Martin 2001). The South BWRO plant consists of the combination of two different plants located in the Southwest Wellfield and receives raw water from 34 production wells (Pearson et al., 2021). The North BWRO plant has 22 groundwater intakes (wells) that tap the Hawthorn Aquifer. The locations of the production wells of both BWRO plants are shown in Fig. 1d.

2.1. Hydrogeological setting of the aquifer system

The geology and hydrogeology of the City of Cape Coral have been described in several publications (Sproul et al., 1972; Boggess 1974; Missimer and Banks 1982; Fitzpatrick, 1986). Additionally, detailed analyses of the geologic and hydrogeologic features of the South and North Wellfields at the City of Cape Coral have been provided by consultant studies (Missimer & Associates, 1985; 1989, 1991; MWH 2007, 2008a, 2008b).

In Southwest Florida, the groundwater system can be grouped into three major hydrogeologic units based on permeability: The Surficial Aquifer System, the Intermediate Aquifer System (or Hawthorn confining unit), and the Floridan Aquifer System (Meyer 1989; Copeland et al., 2010). These three units are composed of a thick sequence of carbonate formations (principally limestone and dolomite), several discrete aquifer systems separated by low permeability "confining" units that generally range in age from Late Paleocene to Early Miocene (Johnston and Bush 1988).

As a water table aquifer, the Surficial Aquifer System in the study area, includes all water-bearing layers from the ground surface to the top of the Hawthorn confining bed and is predominantly comprised of medium to fine-grained sand with varying percentages of shell and calcareous clay (Knapp et al., 1984). These confining beds in the Cape Coral area are relatively thin (9 m) with moderate permeability and intergranular porosity (Wedderburn et al., 1982). Direct precipitation infiltration is the major source of fresh water for the aquifer system.

Within Lee County and in many areas of southwestern Florida, the Hawthorn Aquifer System is subdivided into five poorly defined aquifers

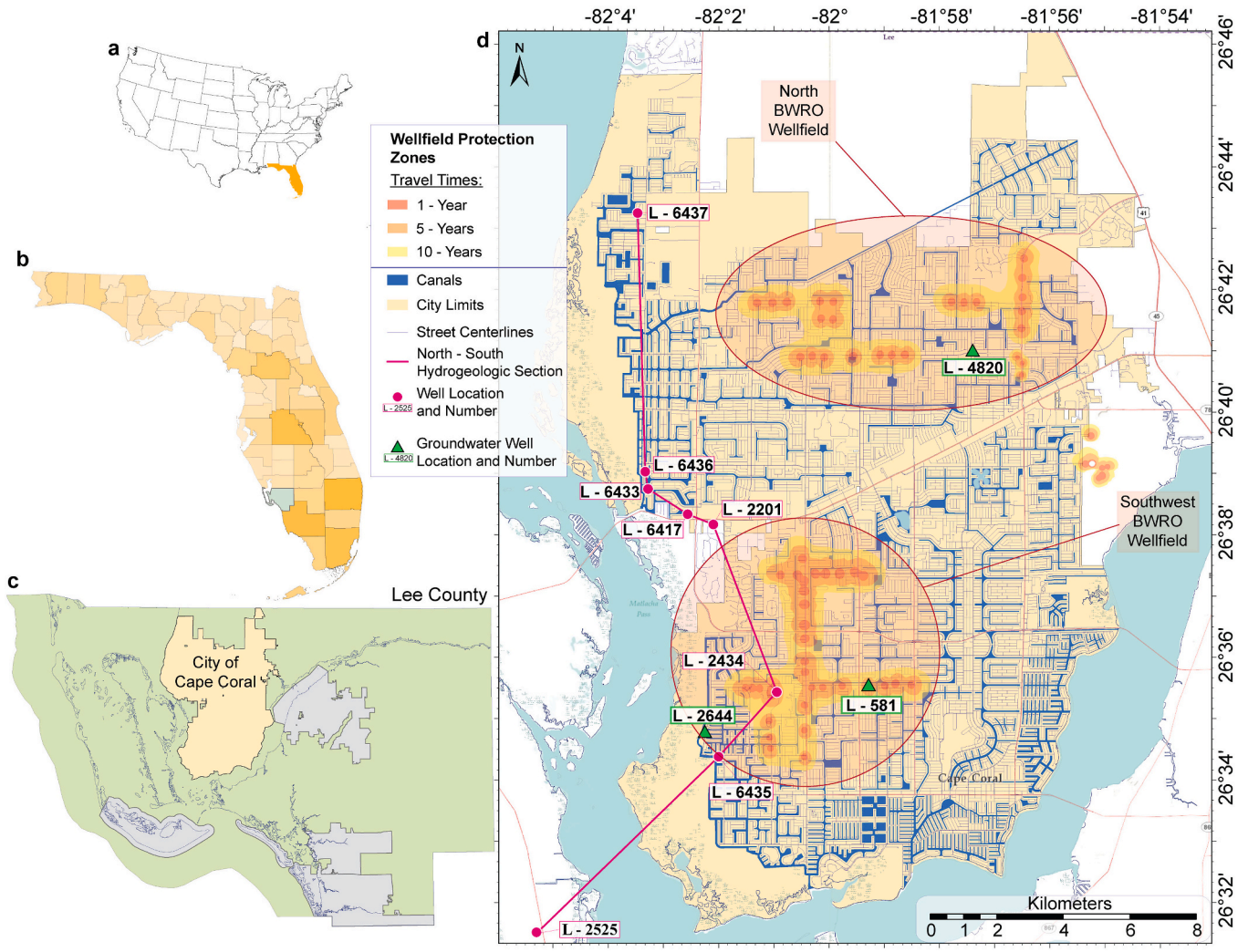

Fig. 1. Cape Coral's peninsula location along the southwest Gulf coast of the U.S. State of Florida. The inset maps (a,b,c) show the location of the study area in southwest Florida. (d) Spatial distribution of groundwater protection (Cone of influence) areas defined based on 1, 5 and 10 years Floridan aquifer system travel time at a 60 mgd pumping rate and represented by red, orange and yellow zones, respectively. Magenta solid line indicates the North-South hydrogeologic section line (see Fig. 2) defined based on well data obtained from USGS (Reese 2003; Missimer et al., 2009; Pearson et al., 2021). The green triangles indicate the location of the groundwater level monitoring wells compared with the InSAR deformation time series. The circles marked in red indicate the primary zones are immediately surrounding production wells of the North and Southwest BWRO facilities. The blue line indicates 640 km-long navigable waterways. (Source: GIS layers and wellfield data obtained from the City of Cape Coral, Florida GIS Open Data Portal, https://capecoral-capegis.opendata.arcgis.com/). (For interpretation of the references to colour in this figure legend, the reader is referred to the Web version of this article.)

that consist of sandy, phosphatic, calcific and dolomitic limestones. Zones of water extraction within this aquifer comprise limestone, calcareous quartz sand, sandstone, and dolomite (Knapp et al., 1984). Only four of these five zones of the Hawthorn formation are present beneath the City of Cape Coral: in descending order, Mid-Hawthorn confining zone, Mid-Hawthorn aquifer, Lower Hawthorn confining bed and Lower-Hawthorn aquifer (Fig. 2). The Mid-Hawthorn confining zone is wholly part of the upper clastic unit of the Hawthorn Formation. It has a very low permeability due to its fine grain size and dense packing arrangement of its matrix component. The Mid-Hawthorn aquifer is mainly composed of sandy, phosphatic limestones and dolomites and interbedded with clayey sand, which lowers the overall transmissivity of the aquifer. This makes the slope of the depression cone around the individual wells quite steep with a small areal extent (Wedderburn et al., 1982; Knapp et al., 1984). This aquifer does not receive any direct recharge from precipitation. The recharge to the Mid-Hawthorn aquifer occurs through vertical leakage across the confining lower and upper aquifers and lateral inflow from adjacent areas (Bush and Johnston, 1988; Berndt and Katz, 1992). The Lower Hawthorn confining bed separates Mid-Hawthorn aquifer from Floridan Aquifer System. It mainly consists of sandy, phosphatic and poorly indurated low permeability limestones resulting from fine-grained composition. Beneath the southwest BWRO wellfield in the Cape Coral and adjacent areas lie the porous limestones near the base of this confining zone, which is sandwiched between layers of low-permeability sediments. These sediment layers act as a barrier to the vertical flow of water from overlying and underlying aquifers (Knapp et al., 1984). The Suwannee Aquifer System is separated from Lower Hawthorn Aquifer by less permeable Suwannee confining beds comprised of calcareous clay and limestone. Lithologically, the Suwannee aquifer is composed of calcarenitic limestone and sandstones with high porosity and permeability.

3. InSAR data and methodology

3.1. InSAR data set

The Terrain Observation with Progressive Scan (TOPS) mode of the Sentinel-1 satellites represents a significant advantage compared to

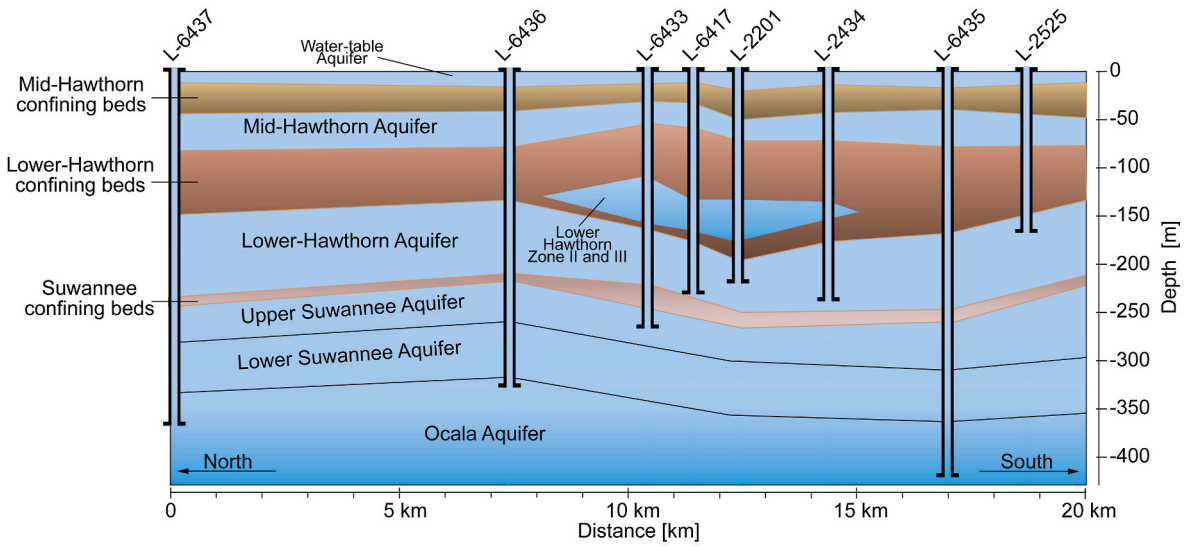

Fig. 2. North-South hydrogeologic cross-section through the City of Cape Coral showing the aquifer and confining bed locations (Pearson et al., 2021).

other sensors' modes, as it provides wide-area coverage and a short revisit time of up to 6-days over Europe and 12-days globally. Here, we used two C-band data sets, with a total of 305 images, from two tracks of the Sentinel 1A/B satellites operated by the European Space Agency, acquired in TOPS mode only along ascending orbits (Track 48 and 121). Data span the period from mid-2015 until April 2022. The City of Cape Coral is entirely covered by the two tracks. The region examined here is completely urbanised with a flat topography, providing favourable phase coherency for interferometric SAR processing.

3.2. InSAR processing

InSAR processing was done using the GSAR-GTSI processing system used by the Norwegian Ground Motion Service (Dehls et al., 2019). The processing system follows the general principles of Persistent Scatterer Interferometry (Crosetto et al., 2016), optimised for wide-area-processing (WAP). Image coregistration is performed using a version of the Enhanced Spectral Diversity algorithm (Prats-Iraola et al., 2012). We used the Shuttle Radar Topography Mission (SRTM) 3-arcsecond digital elevation model to adjust the topographic contribution to the radar phase. All interferograms were computed based on a single master network for PSI analysis. The choice of the master images minimised the spatial and temporal baselines. Atmospheric Phase Screen (APS) is estimated over multiple bursts. All pixels are analysed and tested as potential measurement points, excluding spatially significant water bodies, layover, shadow, and very low mean amplitude. The final measurement point (Persistent Scatter, PS) selection is based on thresholding the achieved RMS deviation from a fitted third-order polynomial + seasonal model, followed by redundancy reduction. Such a low-order polynomial model is more realistic than a linear model without the risk of overfitting.

3.3. Elastic dislocation modelling

Various physical models have been proposed to calculate associated ground subsidence and compaction in the medium across a wide range of aquifers as well as oil and geothermal fields (Trugman et al., 2014; van Thienen-Visser et al., 2015, Fernandez et al., 2018, Métois et al., 2020, Sireci et al., 2021). Analytical solutions for tensile dislocations, as described by Okada (1985), can serve as first-order models for the deformation of a surface caused by buried volumetric or pressure changes in the simplest case of elastic behaviour. Subsidence due to compaction of confined sediments resulting from reservoir draining can be modelled by negative opening (i.e., volume loss or compaction) along the surface of the confining unit (Métois et al., 2020; Sireci et al., 2021). With a given subsiding geometry, determining the subterranean volume change is a linear inverse problem. For every observation point p, the problem can be written as (Maerten et al., 2005)

$$d_p = G^{e,p}\, m^e + E \quad (1)$$

where d_p is the mean velocity at ground point (p), m^e the negative opening on the subsiding element e, $G^{e,p}$ the Green's functions that describe how fixed triangular elements produces displacement at the Earth's surface and E is the observational error. In the inversion process, we search for a solution that simultaneously minimises the L-2 norm of data misfit and the model roughness.

For modelling, we used Poly3Dinv software (Maerten et al., 2005), a 3D-boundary element method with triangular dislocations in a linear-elastic and homogeneous half-space and a damped least-square minimisation (Thomas, 1993). A horizontal surface with triangular elements is constructed at a depth of 50 m that represents the confining unit above the Mid-Hawthorn Aquifer. The size of the triangular element is designed to be 250 m below the subsiding area and up to 1000 m outside of it so that the gradient of subsidence can be mimicked with opening. We decimate the LOS velocity fields on regular grids to balance the number of PS points for computational efficiency and optimal approximation of the actual LOS displacements. The average mean velocity fields of all PS points falling within each grid is then assigned to the centre point of the resulting cell. In order to have a similar decimation pattern with the model surface, the grid sizes are arranged as 200 m in the centre and 500 m outside the subsiding lobe.

3.4. Wavelet analysis

Wavelet analysis is a widely used method for interpreting land subsidence time series and understanding the relationships between observed displacement and its underlying causes (Tomás et al., 2020; Burnol et al., 2021). We used various wavelet tools, namely Continuous Wavelet Transform (CWT), Cross Wavelet Transform (XWT) and Wavelet Coherence (WCT), to analyse the physical relationship between piezometric level change and land subsidence time series. We utilized the Matlab wavelet coherence toolbox provided at http://www.glaciology.net/wavelet-coherence (accessed on 7 December 2022). The CWT is an alternate approach to the classical Fourier analysis for analysing individual time series in the time-frequency domain and is suited to identifying localised intermittent periodicities (Grinsted et al., 2004).

It transforms time-series into an image of spectral power in the time-frequency space allowing oscillations to be visualised in a highly intuitive way.

Similarly, XWT and WCT help identify the common power and relative phase between two time-series that are expected to be related (Tomás et al., 2016). The Cross Wavelet Transform (XWT) tool combines two independent CWTs by multiplying the CWT of one time-series by the complex conjugate of the CWT of the second time-series and exposes regions with high common wavelet power and relative phase in time-frequency space (Grinsted et al., 2004). Wavelet Transform Coherence (WTC) technique permit the evaluation of the coherence between both signals. For detailed information, refer to Grinsted et al. (2004). For wavelet analysis, the time-series input data must be evenly spaced in time. The groundwater monitoring wells used in this study register groundwater levels automatically daily. On the other hand, Sentinel-1 satellites have a regular revisit time of 6 days. The missing or excluded values in both time series are linearly interpolated using a constant time interval. To have the same time sampling interval in both time-series, we down-sampled the daily groundwater level data to the revisiting time period of the used satellite. The linear trends from both datasets have been removed before wavelet analysis by means of a linear least square fitting.

3.5. Aquifer compressibility estimation

The aquifer compressibility refers to the ability of an aquifer, or a layer of water-bearing rock or soil, to change its volume in response to changes in effective stress (Freeze and Cherry, 1979). It is typically measured in terms of the change in volume of an aquifer per unit change in pressure. According to Geertsma (1973), surface subsidence is directly related with the formation thickness, depth, decrease in aquifer pressure, and rock compressibility. To calculate the compressibility of the aquifer that experienced compaction due to a decline in water levels, we used InSAR-measured ground subsidence and changes in well head pressure during a six-year observation period. An aquifer's compressibility can be defined as:

$$\alpha = -\frac{dV_T}{d\sigma_e V_T} \tag{2}$$

Where V_T is the total volume of the aquifer, $d\,V_T$ its temporal evolution, and $d\sigma_e$ is the change in effective stress in the aquifer (Freeze and Cherry,1979). An increase in effective stress $d\sigma_e$ produce a reduction $d\,V_T$ in total soil mass volume. Recall that the total volume of the aquifer consists of the volume of the solids and water-saturated voids. We considered an increment of drawdown, $d\,V_w$, due to the pumping of water in the aquifer that induces an increment of subsidence at the surface, $d\,S_u$, related to the reservoir compaction.

$$\frac{dV_T}{V_T} = -\frac{dS_u}{b} \tag{3}$$

where b is the thickness of the aquifer, taken here as equal to 25 m. The change in effective pressure is:

$$d\sigma_e = \rho_w g dV_w \tag{4}$$

where $\rho_w = 1000\ \mathrm{kg\ m^{-3}}$ and $g = 9.81\ \mathrm{m\ s^{-2}}$ are the density of water and the constant of gravity, respectively. The compressibility can be calculated as:

$$\alpha = \frac{dS_u}{b\rho g dV_w} \tag{5}$$

Where $d\,S_u$ is drawdown of the well head pressure and $d\,V_w$ is the surface subsidence.

4. Results

4.1. Mean line-of-sight velocity fields

Fig. 3 shows the InSAR-derived mean line-of-sight velocity fields calculated from PSI analysis covering the whole City of Cape Coral. The LOS velocities are obtained mostly over the settlements and engineering structures where coherence is relatively high for PSI analysis. The velocity fields of both ascending tracks exhibit similar spatial and temporal deformation patterns.. The small differences in the deformation fields result from local incidence angles, as they are slightly different for the two image sets. The areas with green colour indicate stable regions, whereas warm colours from yellow to red show regions away from the satellite. The wetlands on the west coast of the city and the large cadastral plots to the north have low coherence as they contain few phase-stable targets such as rooftops, rock outcrops, and motorways. Thus no permanent scatterers were found in the time series processing in those areas.

The LOS mean velocity fields show a NE-SW oblong subsidence lobe in the northern part of the city that extends for approximately 100 km^2. The max subsidence rate at the centre of the subsiding lobe is ~32 mm/year in the line-of-sight direction. The overall subsidence pattern in the study area shows an evident spatial correlation with the distribution of the production wells across the north BWRO wellfield. This correlation suggests that surface subsidence is being driven by the abstraction of groundwater as a feedwater source to the BWRO plant.

4.2. Compaction modelling

Compaction induced by groundwater pumping is most pronounced in clays, far more compressible than sands, which are effectively squeezed during persistent overexploitation of the surrounding aquifer (Fernandez et al., 2018; Murray and Lohman, 2018). We modelled the compaction of confined sediments resulting from a dropdown of the groundwater table by negative opening (i.e., volume loss) using the 3-D boundary element method described in section 3.3. We use the surface velocity fields in LOS direction obtained from both ascending InSAR datasets to perform a regularised, least square inversion for the source volumes. The subsidence distributions inverted from both InSAR datasets agree with each other as there is an excellent spatio-temporal consistency between both tracks (see Fig. 4). Modelling results show that subsidence between 2014 and 2022 in the Northern well field and its vicinity in Cape Coral gives rise to a net rate of volumetric deflation of ~ 0.67 $Mm^3\ yr^{-1}$ due to compaction of the confining layer.

5. Discussion

5.1. Spatio-temporal variability of subsidence

Hydraulic head levels from observation wells in both wellfields provide direct measurements of the fluid pressure at depth. The observation well data showing regional groundwater level trend is provided by the U.S. Geological Survey (USGS). Using piezometric data, we can better constrain the hydrogeological mechanism that produces the observed subsidence. Only two wells at Cape Coral were suitable for comparison with InSAR-derived ground deformation, one in the north (L-4820) and one in the south (L-581) wellfield.

Fig. 5 shows the temporal evolution of ground deformation at selected locations across both wellfields. The analysed displacement time series are represented by the average accumulated displacement of the PS points falling within the 100 m radius buffer zone surrounding the wells. As seen in Fig. 5a, PSI time series calculated from both tracks show an overall linear trend of ground subsidence in the north wellfield. The groundwater level also shows a linearly decreasing trend with a distinct seasonal variation. Twenty-two production wells in this region supply feed water to the North BWRO facility, which was brought online

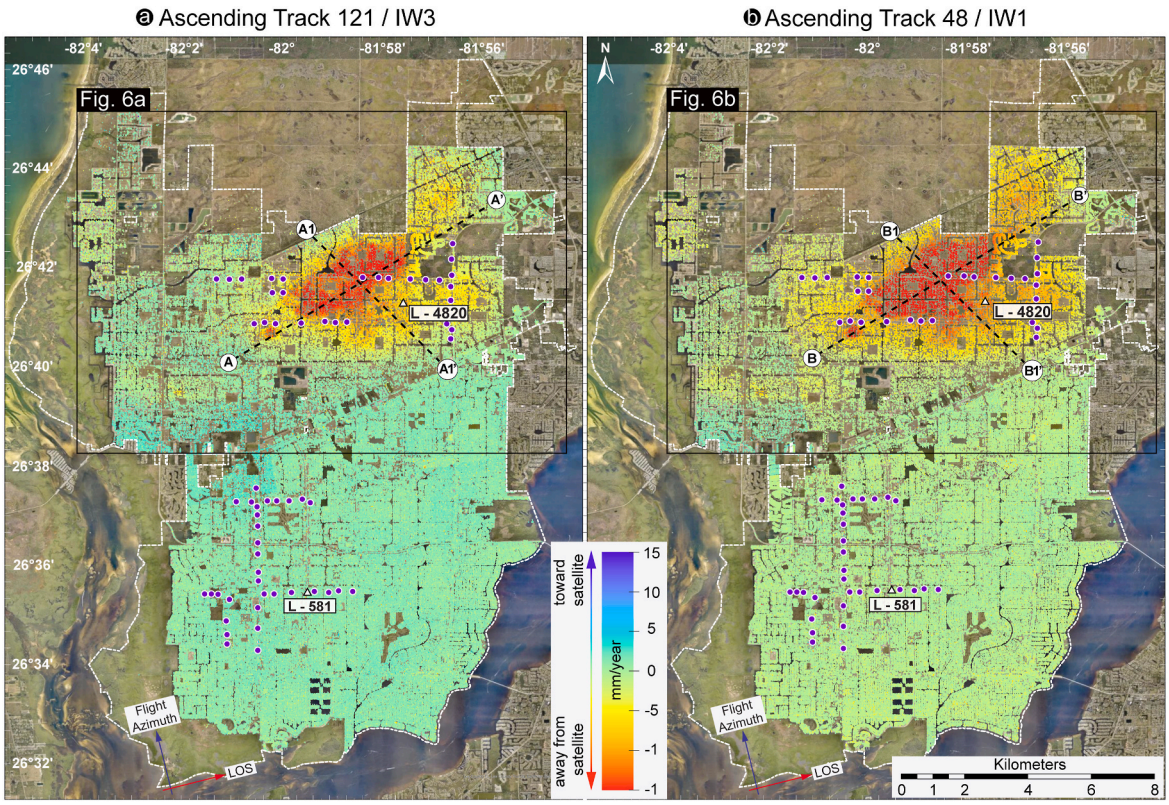

Fig. 3. Mean line-of-sight (LOS) velocity fields for the period 2015–2022, from Sentinel 1A and 1B ascending tracks 121(a) and 48(b), obtained from PSI time series analysis. Negative velocities (cold colours) represent the motion of the ground toward the satellite, and positive velocities (warm colours) represent motion away from the satellite. Purple points represent the production well locations in the North and Southwest wellfields. White dashed lines indicate the boundary of the City of Cape Coral. The blue and red arrows show the line-of-sight and flight directions of the satellite for the data used in this study. (For interpretation of the references to colour in this figure legend, the reader is referred to the Web version of this article.)

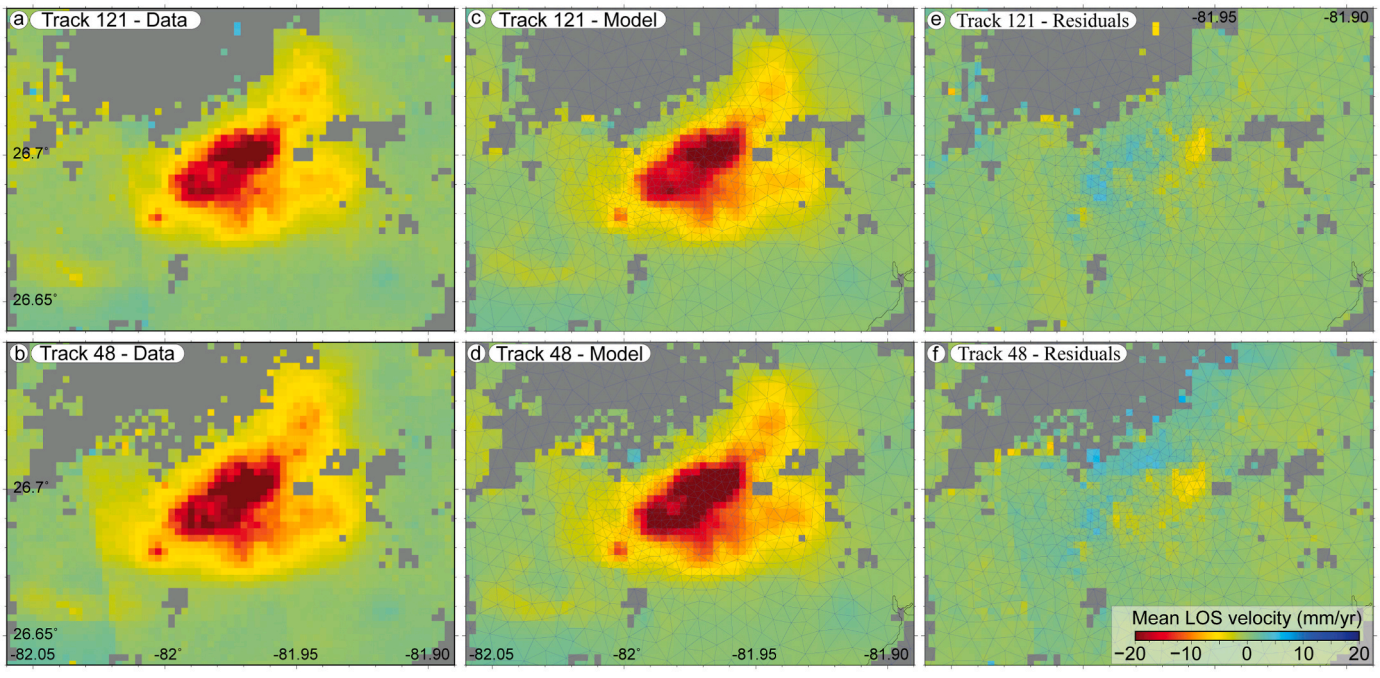

Fig. 4. Modelling subsidence with the Poly3D boundary element method. The subsidence is modelled with negative opening (i.e., volume loss) on near horizontal plane that represents the confining unit above the Mid-Hawthorn Aquifer at a depth around 50 m.

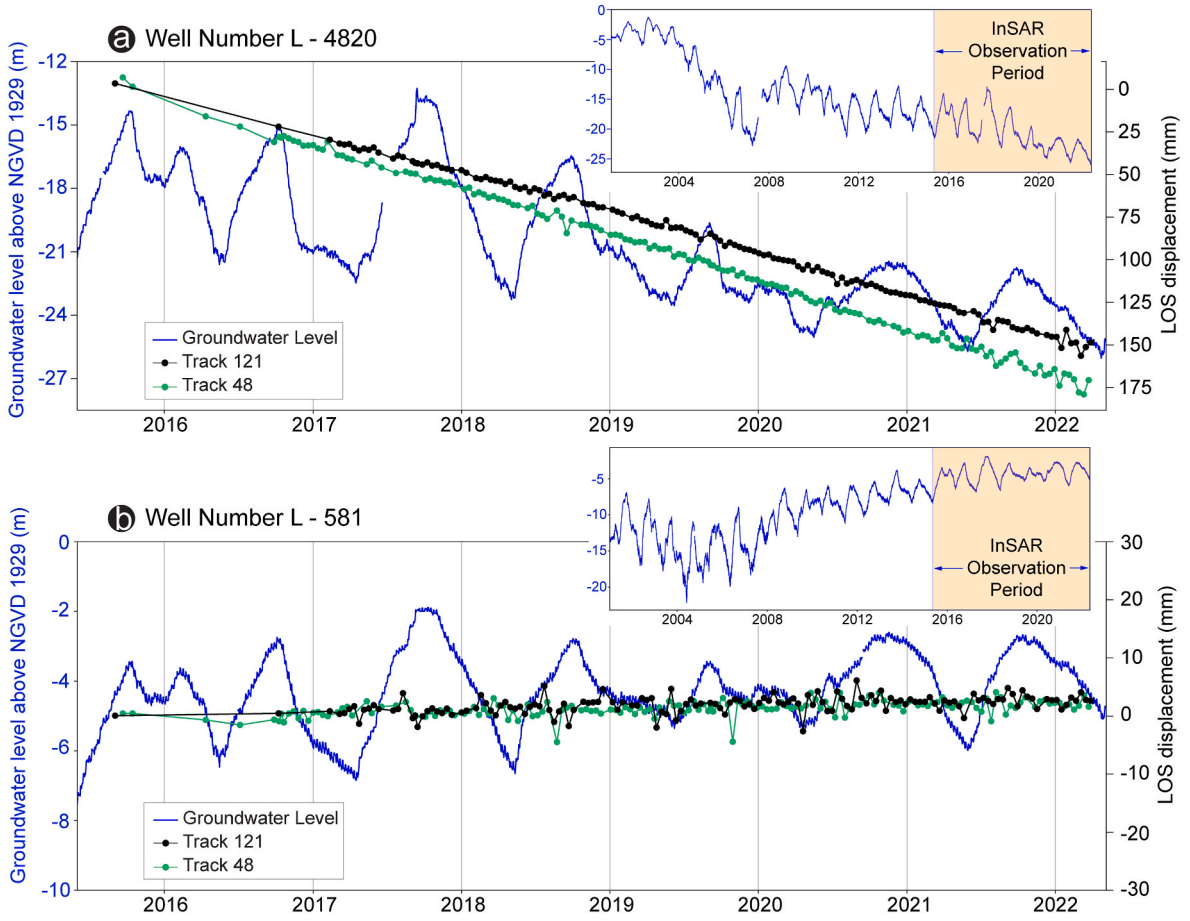

Fig. 5. Temporal evolution of the subsidence of selected points around the groundwater monitoring wells L-4820 (a) and L-581 (b) located within the north and southwest BWRO well fields, respectively. The well locations are shown in Fig. 1. The groundwater data is obtained from U.S Geological Survey, National Water Information System. The inset graphs show groundwater level fluctuations of both monitoring wells for the last two decades To better quantify the spatio-temporal evolution of the subsidence pattern over the northern wellfield, we took 50-m-thick swath profiles along the major (A-A′ and B–B′) and minor axes (A1-A1′ and B1–B1′) of the NE-SW oblong subsidence lobe presented in Fig. 3a and b. Fig. 6 indicates ground subsidence is characterised by a persistent motion with a very linear behaviour, gradually decreasing with the distance to the production wells. Looking at this subsidence pattern obtained from two ascending tracks along two perpendicular profiles highlights excellent consistency between both tracks. The observed surface deformation pattern being nearly symmetrical and the centre of the active northern wellfield having a strong correlation with high subsidence rates suggests that the local subsidence is being influenced by reservoir compaction, similar to what has been observed in other areas (Liu et al., 2015; Métois et al., 2020).

in March 2010. The groundwater level has dropped at a pace of roughly 1 m per year since then (See the inset graph in Fig. 5a). Therefore, as its trend is approximately linear over a decade, we assume that the BWRO facility extracts a large amount of groundwater with a relatively linear trend. On the other hand, following the activation of the Northern BWRO facility in 2010, extensive maintenance, repairs and retrofits at the 39-year-old Southwest BWRO plant were initiated. As a result, the pumping rates in most of the production wells have significantly dropped, and some wells were out of service because of high concentrations of chloride being encountered or maintenance (Pearson et al., 2021). Because of this, the groundwater level has been rising back to its natural level, a process known as water table rebound (Colombo et al., 2017), during the last two decades (inset graph in Fig. 5b). During the observation period of 2015–2022, PSI velocity fields demonstrate overall stability across the southern section of the city spatially (Fig. 3a and b) and temporally (Fig. 5b).

The correlation between the pattern of subsidence and production well distribution in the Northern well field, along with the constant rate of subsidence, suggests that subsidence is primarily caused by pressure loss in the shallow aquitard due to over-extraction of groundwater. The subsidence time-series characterised by a steady linear trend also implies a long-term inelastic compaction in the shallow clay and silt rich aquitard. Despite the significant seasonal decrease in piezometric level, a quasi-stable subsidence trends were previously observed in a limestone aquifer in Konya, Turkey, using satellite interferometry (Caló et al., 2017). On the other hand, the same study reported a strong seasonal correlation between piezometric level change and ground deformation over the alluvial sediments characterised by high compressibility (Caló et al., 2017). Similar inelastic permanent subsidence have also been reported elsewhere e.g. in Beijing, China (Gao et al., 2016), Mexico City (Cigna F. & Tapete, D, 2022), Tehran, Iran (Haghshenas Haghighi and Motagh, 2019), New Delhi, India (Garg et al., 2022) and Madrid (Ezquerro, P. et al., 2014) as the aquifer system undergoes a continuous compaction.

All the wells in this region use brackish water extracted from the Lower Hawthorn/Suwannee Zone 1 Aquifer, which is the upper section of the Floridan aquifer system (Missimer and Martin 2001). At least eight distinct aquifers underly the North BWRO wellfield, from the surface down to 1100 m, each with its own potentiometric surface (Harvey and Missimer 2020) and classified as semi-confined or leaky aquifer (Walton 1970). However, because of the very high leakage, it is treated as one aquifer. Therefore, when production wells extract water from the Lower Hawthorn Zone-1 Aquifer, the major recharge is upwards from the underlying aquifer, with each succeeding deeper aquifer

being impacted by the upward movement of water (Harvey and Missimer 2020). This means that the production wells capture a greater amount of regional flow through the aquifer. As a result, the cone of depression in such a semi-confined aquifer might affect a wider area over time until it reaches a stationary state, where the expansion stops. However, when multiple wells are operated simultaneously, such as those in the north wellfield, each forms a unique cone of depression, depending on the discharge of each well. The spatial combination of the wells in the wellfield generates a wider, complex three-dimensional zone of depletion (Custodio and Llamas, 1983). In addition to the aquifer characteristics, the pumping rate in the wells and the positions between multiple wells are the most critical parameters that control the size and shape (slope) of the depletion cone and the corresponding land subsidence pattern. Ground subsidence rates in the wellfield and its surrounding area decrease from the centre of the wellfield, as seen in Fig. 3, depending on the shape of the cone of depression that develops around the wellfield. The cone of depression might be distorted due to the regional heterogeneity of the soils forming the aquifer and confining layer (Budhu and Adiyaman 2009). Since hydraulic conductivity through the aquifer can vary spatially and be influenced by the complex depositional process (Zhu et al., 2017), land subsidence would be uneven, depending on the aquifer's soil type and the potentiometric surface of the groundwater.

5.2. Wavelet-based analysis

The exploration of the CWT visualising the spectral content of the groundwater level change at L4820 reveals a distinct 1-year cycle with interannual fluctuations throughout a 6-year observation period (Fig. 7a) between 2016 and 2022. However, InSAR-derived ground deformation shows a partial yearly cycle with low wavelet power and short-term periodicity of 3–4 months. This is caused by the associated uncertainty in the deformation time series as the amplitude of the observed detrended deformation signal is close to the uncertainty level of the data. The XWT cross analysis of groundwater level change and the mean InSAR displacement in the LOS display the frequency component distribution with time, while WTC shows the coherence of both time series in the time-frequency space. The most significant localised co-varying power between two time series can be observed at a period of one year, the smaller peaks in power spectrum associated with a period between 3 and 4 months are observed (Fig. 7d and e). While the groundwater level is in phase with LOS displacement obtained from track 121, between 2017 and 2021, it is leading the LOS displacement obtained from track 48 within the same period.

Fig. 7f and g shows the Wavelet Coherence between groundwater level change and LOS displacements obtained from track 121 (d) and 48 (e). The WTC analysis presents a localised correlation of about 0.8 (*i.e.,* $0.8 \leq R \leq 0.9$) with varying phase relationships with a period between 3 and 4 months between 2019 and 2022.

5.3. Compressibility and reservoir volume loss

We utilized the approach described in section 3.5 to evaluate the compressibility of the aquifer that was compressed as a result of the reduction in water level. Applied to the northern wellfield, Fig. 5a shows that drawdown ($d\ S_u$) increased 6 m and the surface subsidence ($d\ V_w$) increased 0.2 m during the InSAR observation period of 6 years. As a result, the compressibility is found 1.35 $\bullet 10^{-7}\ Pa^{-1}$ corresponding to typical values for clay sediments (Freeze and Cherry,1979). The compressible soft clay layer and groundwater level are located at the uppermost Mid-Hawthorn confining beds, which provide the lithology and structural background for ground subsidence in the northern wellfield. The compressible clay layer thickness in this area reaches 25–30 m. The aquifer system in the study area comprises sandstone and dolostone unit that shows very little mechanical compaction compared to clay bearing confining unit. However, the confining units have the greatest potential to compact. Therefore, it was hypothesised that the volume reduction and compaction occur at the confining layer.

An elastic model that utilise planar negative tensile dislocations (described in Section 3.3) was used to reproduce the observed ground deformation by mimicking reservoir compaction. The estimated deflation rate was found to be $\sim$ 0.67 $Mm^3\ yr^{-1}$ due to compaction of the confining layer. To accurately determine the net volumetric change, a 3D finite element model of the aquifer that incorporates the physical properties, geometry, pressure history as well as the total volume of the extracted water is required which we do not have access to at the moment.

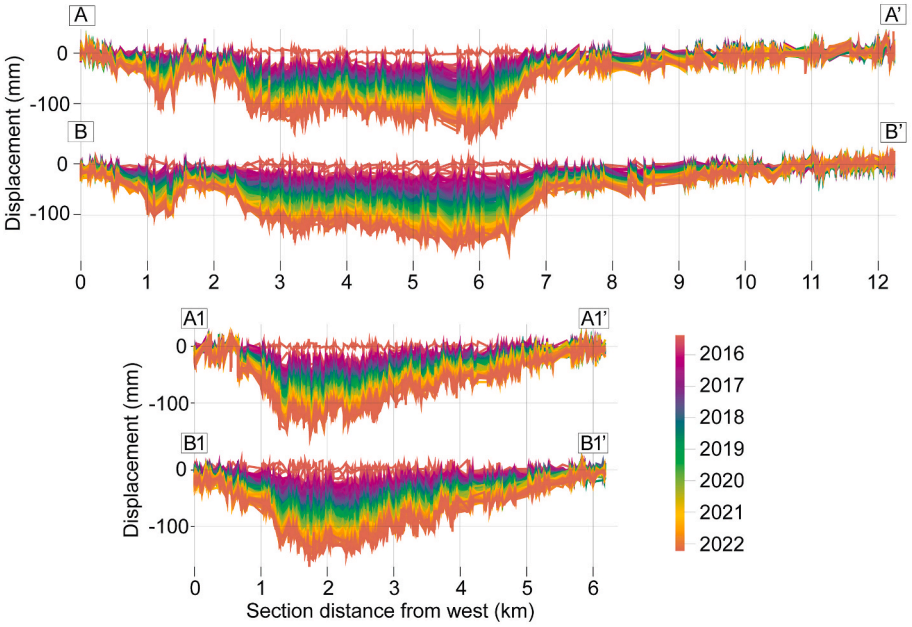

Fig. 6. Profiles of PSI LOS displacement time series (2015–2022) obtained from both ascending tracks 121 and 48 used in this study. The profiles are marked by the 50-m-thick swath profiles along the major (A-A′ and B–B′) and minor axis (A1-A1′ and B1–B1′) of the NE-SW oblong subsidence lobe presented in Fig. 3a and b.

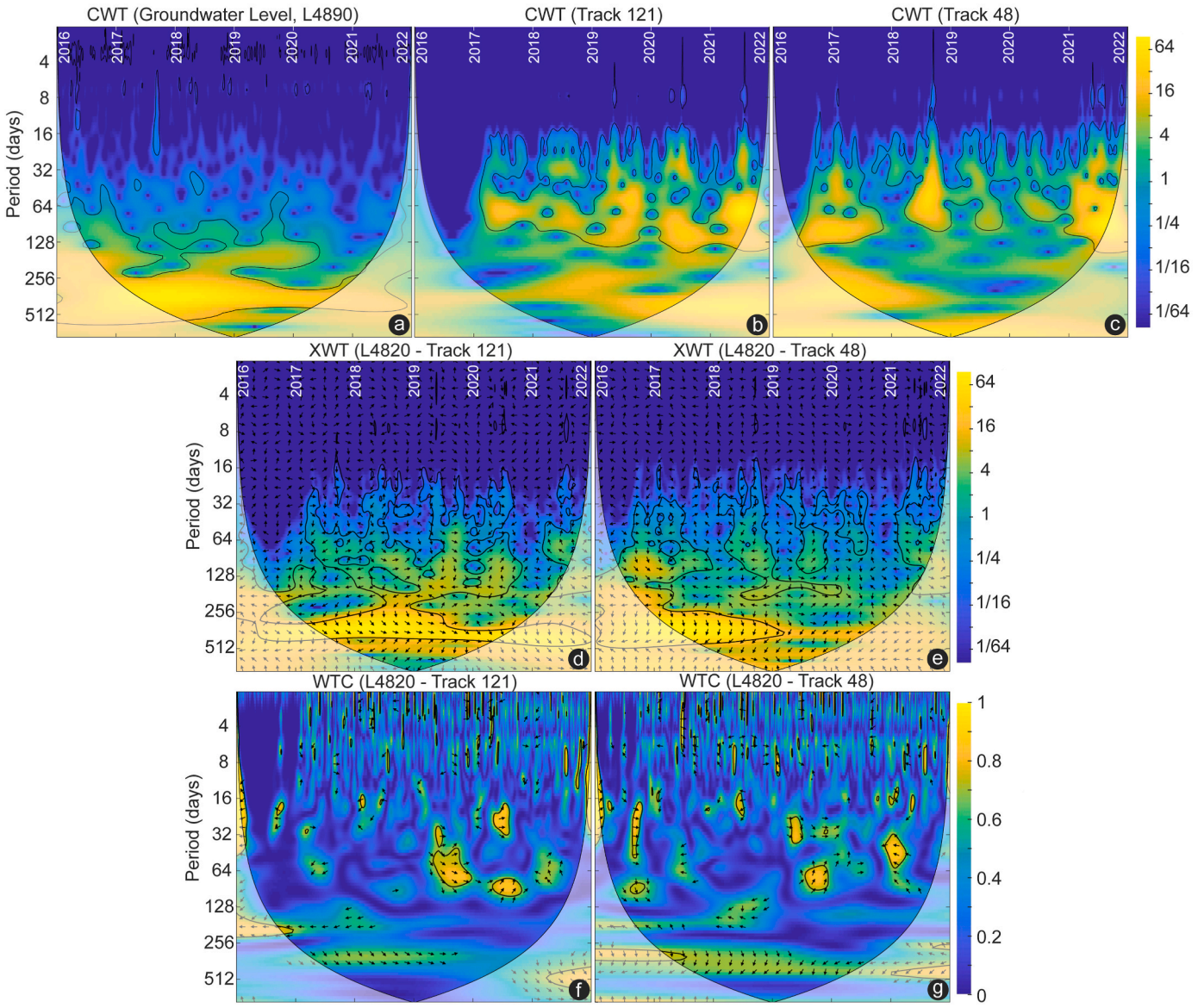

Fig. 7. (**a-c**) Continuous Wavelet Transform (CWT) of the groundwater monitoring well L4820 and InSAR derived subsidence change obtained from track 121 and 48. (**d, e**) The Cross Wavelet Spectrum (XWT) between groundwater level change and both LOS displacements. (**f, g**) The Wavelet Coherence (WTC) between groundwater level change and both LOS displacements. Phase relationship between two time series is shown by the orientation of the arrows in the region of high coherence with in-phase pointing right and anti-phase pointing left. The arrows' tilt up or down indicates the lead-lag relationship between water level and subsidence. The region enclosed by contour line denotes the 5% significant level against red noise. A lighter shadow indicates the cone of influence (COI) where edge effects may affect the image. The blue represent the low power while yellow represents higher power in cross analyses (d–g). (For interpretation of the references to colour in this figure legend, the reader is referred to the Web version of this article.)

5.4. Local depression patterns

Although no local deformation occurs across the city of Cape Coral except for the north BWRO wellfield, we investigated the non-anthropogenic processes governed by the geologic and environmental conditions that may cause ground subsidence. Sinkholes and surficial karstic depressions, as well as caves and disappearing streams, are typical terrain features of Florida's karst landscape. They are generally attributed to the erosional process associated with the chemical weathering and the dissolution of the carbonate rocks within the Floridan aquifer system. To identify non-anthropogenic factors that might potentially contribute to subsidence, we have analysed the distribution of the ancient circular depression represented by lakes and marshes that dot the whole city of Cape Coral. Traditionally, morphometric characteristics of a large number of sinkholes in karst terrain can be derived using topographic models and historical air photographs (Gutierrez et al., 2008; Galve et al., 2009). Recently, very high-resolution digital elevation models (DEMs) derived from Airborne Laser Scanning (LiDAR) have been employed for the 3D characterisation of sinkholes in diverse karst landscapes with high morphological details (Kobal et al., 2015; Filin et al., 2011; Kim et al., 2019). However, since the city's natural drainage pattern and wetland surface topography have been completely transformed by digging canals to provide dry ground for residential use (Stroud 1991), LiDAR-derived high-resolution DEM (0.30 m) cannot provide any information (Fig. 8a) about the closed surface depressions. Therefore, we used historical aerial imagery from 1953, captured before the massive land development project began. The aerial photos show ancient circular and near-circular depressions represented by lakes and marshes that may reveal a long history of sinkhole formation.

The delimitation of the karst-enclosed depressions was done

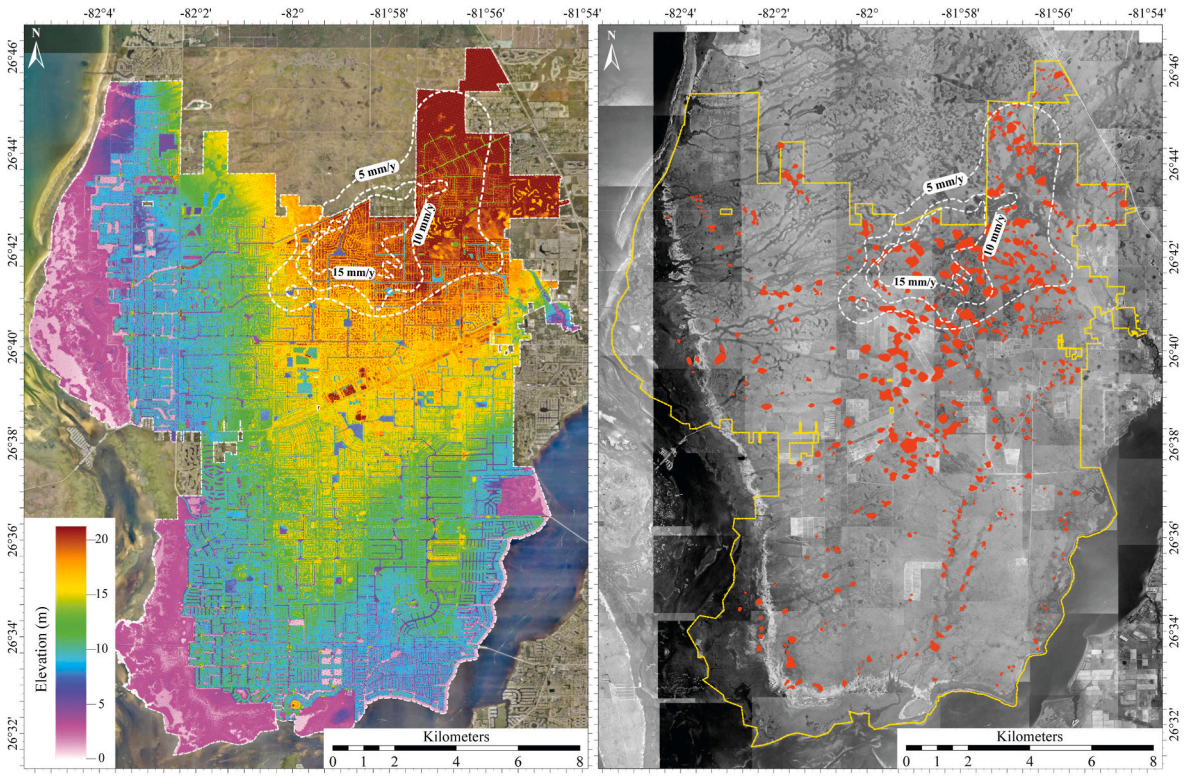

Fig. 8. (a) Airborne LiDAR-derived digital elevation model (DEM) from 2018 and (b) historical aerial imagery from 1953 of the study area overly with 5 mm/yr interval contour map of InSAR-derived subsidence. Both data are obtained from the Lee County, Southwest Florida GIS Portal.

manually. Fig. 8b shows the distributions of clustered depressions and elongated uvalas resulting from the enlargement and coalescence of dolines. InSAR velocity maps (Fig. 3) indicate stability over the depressions, particularly in the southern part of the city. Considering that only a few sinkholes were reported at Cape Coral, compared to the sinkhole epidemic occurring in west central Florida (Tihansky, 1999; Talib et al., 2022), the ground subsidence triggered by sinkhole formations are less expected over the study area. This might suggest that the observed subsidence in the north wellfield is totally modulated by the operation of the desalination plant without any or negligible contribution of dissolution of carbonate rocks.

6. Conclusions

The InSAR-derived subsidence maps presented in this study have significant implications for mitigating hazards relating to land subsidence and may support water resources management at local and regional levels. The comparison of InSAR-derived subsidence maps with the groundwater level in BWRO wellfields demonstrates that groundwater pumping for feeding the Brackish-Water Reverse Osmosis (BWRO) desalination facilities is the primary factor responsible for land subsidence in the northern part of the city. Although the InSAR observations reveal subsidence in the north of the city since 2015, when the long-term groundwater decline and BWRO plant's production activities are considered, it seems likely that the subsidence has been ongoing for the last two decades. Our observations reveal for the first time that a NE-SW elliptical-shaped subsidence lobe in the northern part of the city of Cape Coral extends for approximately 100 km^2 with a maximum annual rate of 32 mm/yr in line-of-sight direction for the 2015–2022 time period. Using piezometric records surrounding both north and southwestern BWRO wellfields, we have presented evidence implying that such deformation likely results from overusing the aquifer system. As groundwater levels have remained relatively stable in the southeast wellfield, little subsidence is shown in the InSAR velocity field. Such absence of ground deformation and water table rebound during the last two decades in the southeast wellfield might imply that the deformation is primarily controlled by elastic compaction that recovers when the groundwater level rises back to its natural level.

Considering the karstic terrain of the study area, with dense depressions and widespread sinkhole activity, our study suggests that aggressive groundwater pumping might potentially facilitate natural sinkhole formation processes. More detailed studies based on systematic detection of sinkhole activity using high-resolution SAR data and LiDAR, as well as geophysical imaging, are required to better assess sinkhole hazards.

This study also shows that the InSAR technique can be used as a robust tool for detecting the drainage areas of the wellfield principally controlled by the volume of withdrawn fluid, aquifer characteristics and positions of multiple wells. Thus, InSAR can be effectively used as an active data source during production and injection, providing crucial information about aquifer heterogeneity, flow paths and sweet spots for new production wells.

Author contributions

Conceptualisation: Gökhan Aslan; Formal analysis and investigation: Gökhan Aslan, Ziyadin Cakir; Writing - original draft preparation: Gökhan Aslan; Writing - review and editing: Gökhan Aslan, Ivanna Penna, John Dehls.

Declaration of competing interest

The authors declare that they have no known competing financial interests or personal relationships that could have appeared to influence the work reported in this paper.

Data availability

Data will be made available on request.

References

Amelung, F., Galloway, D.L., Bell, J.W., Zebker, H.A., Laczniak, R.J., 1999. Sensing the ups and downs of Las Vegas: InSAR reveals structural control of land subsidence and aquifer-system deformation. Geology 27 (6), 483–486. https://doi.org/10.1130/0091-7613(1999)027<0483:STUADO>2.3.CO;2.

Aslan, G., Cakir, Z., Lasserre, C., Renard, F., 2019. Investigating subsidence in the Bursa Plain, Turkey, using ascending and descending Sentinel-1 satellite data. Rem. Sens. 11 (1), 85. https://doi.org/10.3390/rs11010085.

Berndt, M.P., Katz, B.G., 1992. Hydrochemistry of the surficial and intermediate aquifer systems in Florida. Waster Resour. Investig. Rep. 91, 4186.

Boggess, D.H., 1974. Saline Groundwater Resources of Lee County, Florida (No. 74). United States Department of the Interior, Geological Survey.

Borisova, T., Cutillo, M., Beggs, K., Hoenstine, K., 2020. Addressing the scarcity of traditional water sources through investments in alternative water supplies: case study from Florida. Water 12 (8), 2089. https://doi.org/10.3390/w12082089.

Budhu, M., Adiyaman, I.B., 2009. Mechanics of land subsidence due to groundwater pumping. Int. J. Numer. Anal. Methods GeoMech. 34 (14), 1459–1478. https://doi.org/10.1002/nag.863.

Burnol, A., Foumelis, M., Gourdier, S., Deparis, J., Raucoules, D., 2021. Monitoring of expansive clays over drought-rewetting cycles using satellite remote sensing. Atmosphere 12 (10), 1262. https://doi.org/10.3390/atmos12101262.

Bush, P.W., Johnston, R.H., 1988. Ground-water Hydraulics, Regional Flow, and Groundwater Development of the Floridan Aquifer System in Florida and in Parts of Georgia, South Carolina, and Alabama (No. 1403-C). U.S. Government Printing Office.

Caló, F., Notti, D., Galve, J.P., Abdikan, S., Görüm, T., Pepe, A., Balik Şanli, F., 2017. Dinsar-Based detection of land subsidence and correlation with groundwater depletion in Konya Plain, Turkey. Rem. Sens. 9 (1), 83. https://doi.org/10.3390/rs9010083.

Castellazzi, P., Martel, R., Galloway, D.L., Longuevergne, L., Rivera, A., 2016. Assessing groundwater depletion and dynamics using GRACE and InSAR: potential and limitations. Ground Water 54 (6), 768–780. https://doi.org/10.1111/gwat.12453.

Chaussard, E., Bürgmann, R., Shirzaei, M., Fielding, E.J., Baker, B., 2014. Predictability of hydraulic head changes and characterisation of aquifer-system and fault properties from InSAR-derived ground deformation. J. Geophys. Res. Solid Earth 119 (8), 6572–6590. https://doi.org/10.1002/2014JB011266.

Cigna, F., Tapete, D., 2022. Land subsidence and aquifer-system storage loss in Central Mexico: a quasi-continental investigation with sentinel-1 InSAR. Geophys. Res. Lett. 49 (15) https://doi.org/10.1029/2022GL098923.

City of Cape Coral, 2019. Annual Consumer Report.

Colombo, L., Gattinoni, P., Scesi, L., 2017. Influence of underground structures and infrastructures on the groundwater level in the urban area of Milan, Italy. Int. J. Sustain. Dev. Plann. 12 (1), 176–184. https://doi.org/10.2495/SDP-V12-N1-176-184.

Copeland, R., Upchurch, S.B., Scott, T.M., Kromhout, C., Arthur, J., Means, G.H., et al., 2010. Hydrostratigraphic Units of Florida. Florida Geological Survey Poster, 16.

Crosetto, M., Monserrat, O., Cuevas-González, M., Devanthéry, N., Crippa, B., 2016. Persistent scatterer interferometry: a review. ISPRS J. Photogrammetry Remote Sens. 115, 78–89. https://doi.org/10.1016/j.isprsjprs.2015.10.011.

Ezquerro, P., Herrera, G., Marchamalo, M., Tomás, R., Béjar-Pizarro, M., Martínez, R., 2014. A quasi-elastic aquifer deformational behavior: Madrid aquifer case study. J. Hydrol. 519, 1192–1204. https://doi.org/10.1016/j.jhydrol.2014.08.040.

Fernandez, J., Prieto, J.F., Escayo, J., Camacho, A.G., Luzón, F., Tiampo, K.F., et al., 2018. Modeling the two-and three-dimensional displacement field in Lorca, Spain, subsidence and the global implications. Sci. Rep. 8 (1), 1–14. https://doi.org/10.1038/s41598-018-33128-0.

Ferretti, A., Prati, C., Rocca, F., 2001. Permanent scatterers in SAR interferometry. IEEE Trans. Geosci. Rem. Sens. 39 (1), 8–20. https://doi.org/10.1109/36.898661.

Filin, S., Baruch, A., Avni, Y., Marco, S., 2011. Sinkhole characterisation in the Dead Sea area using airborne laser scanning. Nat. Hazards 58 (3), 1135–1154. https://doi.org/10.1007/s11069-011-9718.

Fitzpatrick, D.J., 1986. Tests for Injecting, Storing, and Recovering Freshwater in a Saline Artesian Aquifer, vol. 85. U.S. Department of the Interior, Geological Survey, Lee County, Florida. No. 4249.

Florida Department of Environmental Protection, Floridadep, (access: 28 April, 2022), Alternative Water Suppy, Florida Department of Environmental Protection (https://floridadep.gov/water-policy/water-policy/content/alternative-water-supply).

Freeze, R.A., Cherry, J.A., 1979. Groundwater. Prentice-Hall, Englewood Cliffs, New Jersey, p. 604.

Galloway, D.L., 2014. Retrospective of InSAR/DInSAR contributions to hydrogeology by way of bibliographic search. In: 2014 IEEE Geoscience and Remote Sensing Symposium. IEEE, pp. 2637–2640. https://doi.org/10.1109/IGARSS.2014.6947015.

Galloway, D.L., Hoffmann, J., 2007. The application of satellite differential SAR interferometry-derived ground displacements in hydrogeology. Hydrogeol. J. 15 (1), 133–154. https://doi.org/10.1007/s10040-006-0121-5.

Galve, J.P., Gutiérrez, F., Remondo, J., Bonachea, J., Lucha, P., Cendrero, A., 2009. Evaluating and comparing methods of sinkhole susceptibility mapping in the Ebro Valley evaporite karst (NE Spain). Geomorphology 111 (3–4), 160–172. https://doi.org/10.1016/j.geomorph.2009.04.017.

Gao, M., Gong, H., Chen, B., Zhou, C., Chen, W., Liang, Y., et al., 2016. InSAR time-series investigation of long-term ground displacement at Beijing Capital International Airport, China. Tectonophysics 691, 271–281. https://doi.org/10.1016/j.tecto.2016.10.016.

Garg, S., Motagh, M., Indu, J., Karanam, V., 2022. Tracking hidden crisis in India's capital from space: implications of unsustainable groundwater use. Sci. Rep. 12 (1), 1–17. https://doi.org/10.1038/s41598-021-04193-9.

Geertsma, J., 1973. Land subsidence above compacting oil and gas reservoirs. J. Petrol. Technol. 25 (6), 734–744.

Grinsted, A., Moore, J.C., Jevrejeva, S., 2004. Application of the cross wavelet transform and wavelet coherence to geophysical time series. Nonlinear Process Geophys. 11 (5/6), 561–566. https://doi.org/10.5194/npg-11-561-2004.

Gutierrez, F., Cooper, A.H., Johnson, K.S., 2008. Identification, prediction, and mitigation of sinkhole hazards in evaporite karst areas. Environ. Geol. 53 (5), 1007–1022. https://doi.org/10.1007/s00254-007-0728-4.

Haghighi, M.H., Motagh, M., 2019. Ground surface response to continuous compaction of aquifer system in Tehran, Iran: results from a long-term multi-sensor InSAR analysis. Remote Sens. Environ. 221, 534–550. https://doi.org/10.1016/j.rse.2018.11.003.

Hanssen, R.F., 2001. Radar Interferometry: Data Interpretation and Error Analysis, vol. 2. Springer Science & Business Media.

Harvey, N.J., Missimer, T.M., 2020. Impacts of projected changes in feedwater salinity on the City of Cape Coral, Florida north brackish-water reverse osmosis desalination plant operation. Desalination Water Treat. 181, 1–16. https://doi.org/10.5004/dwt.2020.25382.

Hill, C.P., 2012. Florida brackish water and seawater desalination: challenges and opportunities. Florida Water Resour. J. 22–28.

Hu, X., Bürgmann, R., 2020. Aquifer deformation and active faulting in salt lake valley, Utah, USA. Earth Planet Sci. Lett. 547, 116471 https://doi.org/10.1016/j.epsl.2020.116471.

Jafari, F., Javadi, S., Golmohammadi, G., Karimi, N., Mohammadi, K., 2016. Numerical simulation of groundwater flow and aquifer-system compaction using simulation and InSAR technique: saveh basin, Iran. Environ. Earth Sci. 75 (9), 1–10. https://doi.org/10.1007/s12665-016-5654-x.

Johnston, R.H., Bush, P.W., 1988. Summary of the Hydrology of the Floridan Aquifer System in Florida and in Parts of Georgia, South Carolina, and Alabama, vol. 1403. Department of the Interior, U.S. Geological Survey.

Kim, Y.J., Nam, B.H., Youn, H., 2019. Sinkhole detection and characterisation using LiDAR-derived DEM with logistic regression. Rem. Sens. 11 (13), 1592. https://doi.org/10.3390/rs11131592.

Knapp, M.S., Burns, S.W., Sharp, T.S., Shih, G., 1984. Preliminary Water Resource Assessment of the Mid and Lower Hawthorn Aquifers Western Lee County. South Florida Water Management District Technical Publication, Florida, p. 106, 84-10.

Kobal, M., Bertoncelj, I., Pirotti, F., Dakskobler, I., Kutnar, L., 2015. Using lidar data to analyse sinkhole characteristics relevant for understory vegetation under forest cover - case study of a high karst area in the Dinaric Mountains. PLoS One 10 (3), e0122070. https://doi.org/10.1371/journal.pone.0122070.

Liu, P., Li, Q., Li, Z., Hoey, T., Liu, Y., Wang, C., 2015. Land subsidence over oilfields in the yellow river delta. Rem. Sens. 7 (2), 1540–1564. https://doi.org/10.3390/rs70201540.

Llamas, R., Custodio, E., 1999. Aguas subterráneas. Rev. CIDOB Afers Int. 45/46, 35–57.

Maerten, F., Resor, P., Pollard, D., Maerten, L., 2005. Inverting for slip on three-dimensional fault surfaces using angular dislocations. Bull. Seismol. Soc. Am. 95 (5), 1654–1665. https://doi.org/10.1785/0120030181.

Marella, R.L., Berndt, M.P., 2005. Water Withdrawals and Trends from the Floridan Aquifer System in the Southeastern United States, 1950-2000. U.S. Department of the Interior, U.S. Geological Survey, Reston, Virginia.

Métois, M., Benjelloun, M., Lasserre, C., Grandin, R., Barrier, L., Dushi, E., Koçi, R., 2020. Subsidence associated with oil extraction, measured from time series analysis of Sentinel-1 data: case study of the Patos-Marinza oil field, Albania. Solid Earth 11 (2), 363–378. https://doi.org/10.5194/se-11-363-2020.

Meyer, F.W., 1989. Hydrogeology, Groundwater Movement, and Subsurface Storage in the Floridan Aquifer System in Southern Florida, vol. 1403. U.S. Government Printing Office.

Miller, J.A., 1990. Ground Water Atlas of the United States: Alabama, Florida, Georgia, and South Carolina. U.S. Geol Surv Hydrol Invest Atlas.

Missimer & Associates, 1985. Inc. Cape Coral Reverse Osmosis Wellfield Final Construction Report and Operation and Maintenance Recommendations; Consultant's to the City of Cape Coral, ume 3. FL; Missimer & Associates, Inc., Cape Coral, FL, USA.

Missimer & Associates, 1989. Inc. City of Cape Coral Master Water Supply Plan, Phase I Report: Preliminary Assessment of Sources of Water for Future Potable Water Supply in the City of Cape Coral; Consultant's Report to the City of Cape Coral. Missimer & Associates, Inc., Cape Coral, FL, USA, p. 178p.

Missimer & Associates, Inc, 1991. City of Cape Coral Master Water Supply Plan, Phase II Report: Hydrogeology and Hydraulic Solute Transport Model of the Upper Floridan Aquifer System beneath Cape Coral (Florida).

Missimer, T.M., Banks, R.S., 1982. Miocene cyclic sedimentation in western Lee County, Florida. In: Miocene of southeastern United States: Florida Bureau of Geology Special Publication, 25, pp. 285–299.

Missimer, T.M., Martin, W.K., 2001. The Hydrogeology of Lee County, Florida. Geology and Hydrology of Lee County, Florida, p. 91.

Missimer, T.M., Watson, I., Pankratz, T.M., Maliva, R.G., 2009. Water Supply Development, Aquifer Storage, and Concentrate Disposal for Membrane Water Treatment Facilities. ("Tom Pankratz - Google Scholar") Schlumberger.

Moreau, F., Dauteuil, O., 2013. Geodetic tools for hydrogeological surveys: 3D-displacements above a fractured aquifer from GPS time series. Eng. Geol. 152 (1), 1–9. https://doi.org/10.1016/j.enggeo.2012.10.017.

Murray, K.D., Lohman, R.B., 2018. Short-lived pause in Central California subsidence after heavy winter precipitation of 2017. Sci. Adv. 4 (8), eaar8144. https://doi.org/10.1126/sciadv.aar8144.

MWH, 2007. Southwest Wellfield Expansion Well Completion Report; Consultant's to the City of Cape Coral. FL; MWH: Cape Coral, FL, USA.

MWH, 2008a. North Wellfield Expansion Well Completion Report; Consultant's Report to the City of Cape Coral. FL; MWH, Cape Coral, FL, USA.

MWH, 2009. W-2C north production well system, north wellfield completion Report. In: 2008; Consultant's Report to the City of Cape Coral: City of Cape Coral; MWH: Cape Coral, FL, USA.

Okada, Y., 1985. Surface deformation due to shear and tensile faults in a half-space. Bull. Seismol. Soc. Am. 75, 1135–1154.

Pearson, J.L., Hegy, M., Missimer, T.M., 2021. Impacts of feedwater quality change on the oldest continuously operated brackish-water reverse osmosis desalination plant in the United States. Water 13 (19), 2654. https://doi.org/10.3390/w13192654.

Peng, M., Lu, Z., Zhao, C., Motagh, M., Bai, L., Conway, B.D., Chen, H., 2022. Mapping land subsidence and aquifer system properties of the Willcox Basin, Arizona, from InSAR observations and independent component analysis. Remote Sens. Environ. 271, 112894 https://doi.org/10.1016/j.rse.2022.112894.

Pepe, A., Calò, F., 2017. A review of interferometric synthetic aperture RADAR (InSAR) multi-track approaches for the retrieval of Earth's surface displacements. Appl. Sci. 7 (12), 1264. https://doi.org/10.3390/app7121264.

Prats-Iraola, P., Scheiber, R., Marotti, L., Wollstadt, S., Reigber, A., 2012. TOPS interferometry with TerraSAR-X. IEEE Trans. Geosci. Rem. Sens. 50 (8), 3179–3188. https://doi.org/10.1109/TGRS.2011.2178247.

Qu, F., Lu, Z., Zhang, Q., Bawden, G.W., Kim, J.W., Zhao, C., Qu, W., 2015. Mapping ground deformation over Houston–Galveston, Texas using multi-temporal InSAR. Remote Sens. Environ. 169, 290–306. https://doi.org/10.1016/j.rse.2015.08.027.

Reese, R.S., 2003. Hydrogeology and the Distribution of Salinity in the Floridan Aquifer System, Southwestern Florida. U.S. Department of the Interior, U.S. Geological Survey.

Schuite, J., Longuevergne, L., Bour, O., Boudin, F., Durand, S., Lavenant, N., 2015. Inferring field-scale properties of a fractured aquifer from ground surface deformation during a well test. Geophys. Res. Lett. 42 (24), 10–696. https://doi.org/10.1002/2015GL066387.

Short, N.M., Blair, R.W. (Eds.), 1986. Geomorphology from Space: a Global Overview of Regional Landforms.

Sinclair, W.C., 1982. Sinkhole Development Resulting from Groundwater Withdrawal in the Tampa Area. U.S. Geological Survey, Water Resources Division, Florida, pp. 1–19.

Şireci, N., Aslan, G., Cakir, Z., 2021. Long-term spatiotemporal evolution of land subsidence in Konya metropolitan area (Turkey) based on multisensor SAR data. Turk. J. Earth Sci. 30 (5), 681–697. https://doi.org/10.3906/yer-2104-22.

Spencer, T., Altman, P., 2010. Climate Change, Water, and Risk: Current Water Demands Are Not Sustainable. Natural Resources Defense Council, Washington, DC. http://www.nrdc.org/globalWarming/watersustainability/files/WaterRisk.pdf. (Accessed 29 August 2013).

Sproul, C.R., Boggess, D.H., Woodard, H.J., 1972. Saline Water Intrusion from Deep Artesian Sources in McGregor Isles Area of Lee County (Florida).

Stroud, H.B., 1991. Water resources at Cape Coral, Florida: problems created by poor planning and development. Land Use Pol. 8 (2), 143–157. https://doi.org/10.1016/0264-8377(91)90006-5.

Talib, O.C., Shimon, W., Sarah, K., Tonian, R., 2022. Detection of sinkhole activity in West-Central Florida using InSAR time series observations. Remote Sens. Environ. 269, 112793 https://doi.org/10.1016/j.rse.2021.112793.

Thomas, A.L., 1993. POLY3D: A Three-Dimensional, Polygonal Element, Displacement Discontinuity Boundary Element Computer Program with Applications to Fractures, Faults, and Cavities in the Earth's Crust. Master Thesis at Stanford University.

Tihansky, A.B., 1999. Sinkholes, west-central Florida. Land subsidence in the United States: U.S. Geol. Surv. Circular 1182, 121–140.

Tomás, R., Li, Z., Lopez-Sanchez, J.M., Liu, P., Singleton, A., 2016. Using wavelet tools to analyse seasonal variations from InSAR time-series data: a case study of the Huangtupo landslide. Landslides 13 (3), 437–450. https://doi.org/10.1007/s10346-015-0589-y.

Tomás, R., Pastor, J.L., Béjar-Pizarro, M., Bonì, R., Ezquerro, P., Fernández-Merodo, J.A., et al., 2020. Wavelet analysis of land subsidence time-series: Madrid Tertiary aquifer case study. Proceedings of the International Association of Hydrological Sciences 382, 353–359. https://doi.org/10.5194/piahs-382-353-2020.

Trugman, D.T., Borsa, A.A., Sandwell, D.T., 2014. Did stresses from the cerro prieto geothermal field influence the el mayor-cucapah rupture sequence? Geophys. Res. Lett. 41 (24), 8767–8774. https://doi.org/10.1002/2014GL061959.

United States Census Bureau, 2021. https://data.census.gov/cedsci/.

U.S. Geological Survey, 2016. National Water Information System Data Available on the World Wide Web (USGS Water Data for the Nation). https://doi.org/10.5066/F7P55KJN accessed [17 May, 2022], at URL [http://waterdata.usgs.gov/nwis/.

van Thienen-Visser, K., Pruiksma, J.P., Breunese, J.N., 2015. Compaction and subsidence of the Groningen gas field in The Netherlands. Proceedings of the International Association of Hydrological Sciences 372, 367–373. https://doi.org/10.5194/piahs-372-367-2015.

Walton, W.C., 1970. Groundwater Resources Evaluation. McGraw Hill Book Co., New York.

Wedderburn, L.A., Knapp, M.S., Waltz, D.P., Burns, W.S., 1982. Hydrogeologic reconnaissance of lee county, 1. In: Florida: South Florida Water Management District Technical Publication, 82, p. 210.

Zhu, L., Gong, H., Dai, Z., Guo, G., Teatini, P., 2017. Modeling 3-D permeability distribution in alluvial fans using facies architecture and geophysical acquisitions. Hydrol. Earth Syst. Sci. 21 (2), 721–733. https://doi.org/10.5194/hess-21-721-2017.